Nucleation, growth and coalescence of voids in dual phase steels: from model microstructures to microstructure based modeling

A.P. Pierman[1], *C. Tekoğlu*[1], *T. Pardoen*[1], *P.J. Jacques*[1]

[1] *Institute of mechanical, materials and civil engineering, Université catholique de Louvain, Place Sainte Barbe 2, B-1348 Louvain-la-Neuve, Belgium*

E-mail: anne-pascale.pierman@uclouvain.be, pascal.jacques@uclouvain.be

Abstract

Dual phase steels, a composite made of ferrite matrix and hard martensite inclusions, are currently introduced as automotive structural parts owing to their excellent strength/ductility compromise while involving only small amounts of alloying elements. Nevertheless, these alloys suffer sometimes from limited damage and fracture resistance, for instance during forming operations, due to early void nucleation leading to small or moderate fracture strains depending mostly on the characteristics of the martensite phase. Several DP steels, presenting various amounts of martensite and C content, with or without additional tempering, are investigated by performing mechanical tests under different loading conditions, in-situ micromechanical tests, nanoindentation, and in depth damage mechanism characterization. A micromechanical model combining an advanced Gurson model and homogenization theory is validated by comparison to the experimental results and used to perform a comprehensive parameter study with the objective of guiding microstructure optimization.

1. Introduction

One of the major engineering challenges in today's automotive industry is to significantly decrease the weight of the structural components while keeping the same level of reliability. An efficient way of achieving this goal is to use Dual Phase steels, which exhibit an excellent combination of strength and ductility owing to their in-situ composite microstructure, a mixture of finely grained soft ferrite matrix and hard martensite reinforcement [1]. However, in the literature there is limited information on the fracture mechanisms of DP steels, which is crucial for the optimization of the microstructure towards better mechanical properties. Here, some preliminary results obtained on two DP steels containing different amounts of martensite are presented. The final aim of this study is to relate the fracture behavior of DP steels to the amount of martensite and carbon content. Two tempering treatments are carried out to activate the diffusion, and thus to reduce the supersaturation of carbon. The mechanical properties of as-quenched and tempered specimens are characterized by performing tensile tests (stress-strain evolution, fracture strain) and nanoindentation measurements (hardness value). The experimental results for the fracture strain are also compared with the predictions obtained with a new advanced micromechanics-based fracture model.

The processing and testing methods are described in section 2. The experimental results are presented in section 3, and discussed in section 4. The micromechanics-based fracture model is briefly introduced and the predictions of the model are compared with the experimental results, in terms of the fracture strain in section 5.

2. Experimental procedure

The composition of the investigated DP steel is given in Table 1.

C	Mn	Si	P	S	Cr	Ni	Cu	Nb	Al	N
0.17	1.5	0.4	0.013	0.012	0.019	0.027	0.019	0.017	0.03	0.006

Table 1: Chemical composition (in wt. %) of the investigated steel

In the following, DP steels are referred to by different names based on their martensite content and tempering treatments, as given in Table 2. Two different heat treatments were carried out to generate DP steels with distinct microstructures: specimens were hold for 5 min at either 725°C or 750°C before water quenching, leading to DP steels with 20% (M20) or 30% (M30) of martensite, with an estimated C content of 0.85 wt% and 0.56 wt%, respectively. Both as-quenched specimens (AQ, see Table 2), and specimens tempered by holding them either for 30 min at 200°C or 300 min at 300°C (T1 and T2, respectively, in Table 2) were tested. Figure 1 shows the microstructure of a M20-AQ DP steel.

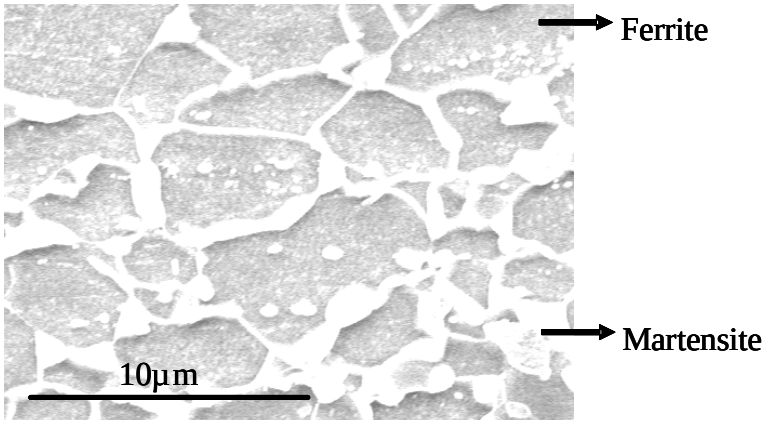

Figure 1: Microstructure of DP steel with 20% of martensite

Samples observed by SEM were first polished with SiC paper followed by 6µm and 1 µm diamond suspensions. The microstructure of the samples was revealed by etching with 2% Nital. The nanoindentation sample preparation followed the same procedure as the SEM sample preparation, but finished by an additional OPS polishing. Indentation tests were performed by using a Berkovitch tip, after calibration of the nanoindentation machine on quartz. Standard dog-bone specimens (with a calibrated length of 100 mm and a width of 1mm) were used for the tensile tests.

M20	Material 1 : Dual Phase steel with 20% of martensite
M30	Material 2 : Dual Phase steel with 30% of martensite
AQ	As Quenched
T1	Tempering 1 : 30min at 200°C
T2	Tempering 2 : 300min at 300°C

Table 2: denomination of the different steels in the paper

3. Experimental results

The true stress-true strain curves shown in Fig. 2 clearly point out the dependence of the mechanical properties of DP steels on the martensite content and on tempering. The yield strength of the samples with a 30% of martensite (M30) is larger than the yield strength of samples with 20% of martensite (M20). Uniform strain, on the other hand, shows an opposite tendency and slightly decreases with increasing martensite volume fraction. After tempering, Lüders plateau appears on the stress-strain curves and the plateau strain ($\Delta\varepsilon$) is larger for T2 conditions, which is the tempering with high temperature and long time (see Table 2).

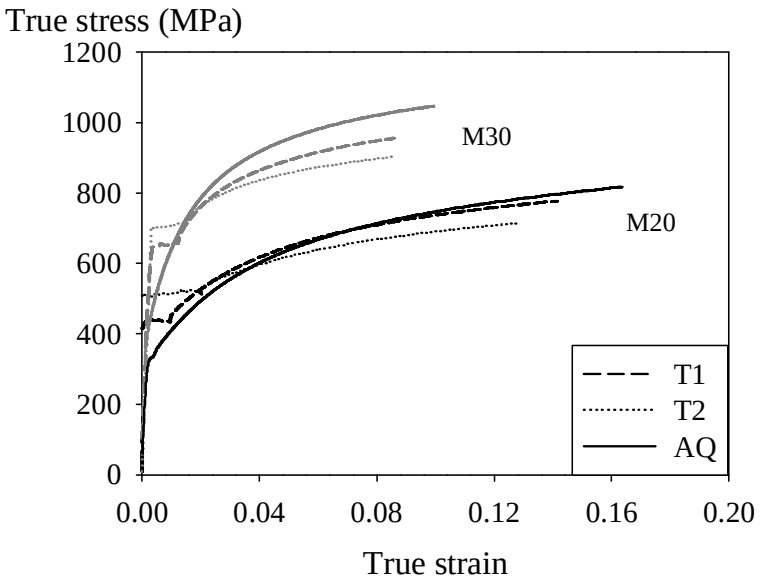

Figure 2: True stress-true strain curves of the 6 DP steels

Figures 3a and b (3c and d) show the hardness of martensite (ferrite) measured by nanoindentation with three different applied loads. The hardness of martensite, which decreases with increasing load due to the size effects and, probably, "substrate" effects, is high for the as-quenched samples and significantly decreases with tempering (see Figs. 3a and b). The effect of tempering on the hardness of martensite depends on the C content: the decrease in hardness after treatment T1 is smaller for steel M30 than it is for steel M20, in which the martensite C content is larger. Condition T2, on the other hand, considerably reduces the hardness of steel M30, while keeping the hardness of steel M20

unaffected, compared to the hardness values obtained by treatment T1 (see Figs. 3a, b). Figures 3c and d show that the evolution of the hardness of ferrite is different from martensite, with a constant level independent of the tempering conditions. Figure 4 shows the effect of tempering on the fracture strain ε_f, which is estimated using

$$\varepsilon_f = \ln\left(\frac{A_0}{A_f}\right), \tag{1}$$

with A_0 and A_f being the initial and final cross-sectional area, respectively. It is worth noting that A_f is measured on SEM micrographs. Figure 4 shows that tempering increases the fracture strain of DP steels, the improvement being larger for the condition T2.

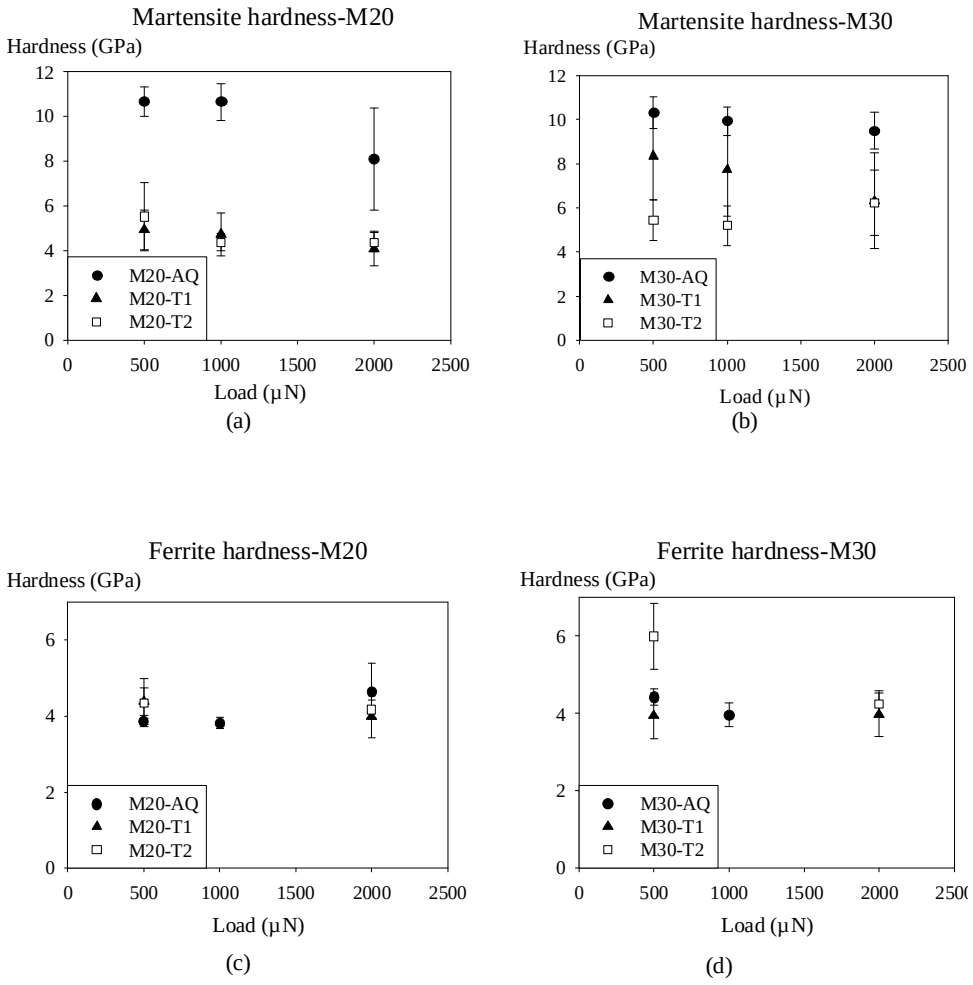

Figure 3: Nanoindentation hardness of martensite and ferrite in steel M20, (a) and (c), respectively, and in steel M30, (b) and (d), respectively, plotted versus applied load, for as-quenched (AQ) and tempered (T1 and T2) conditions .

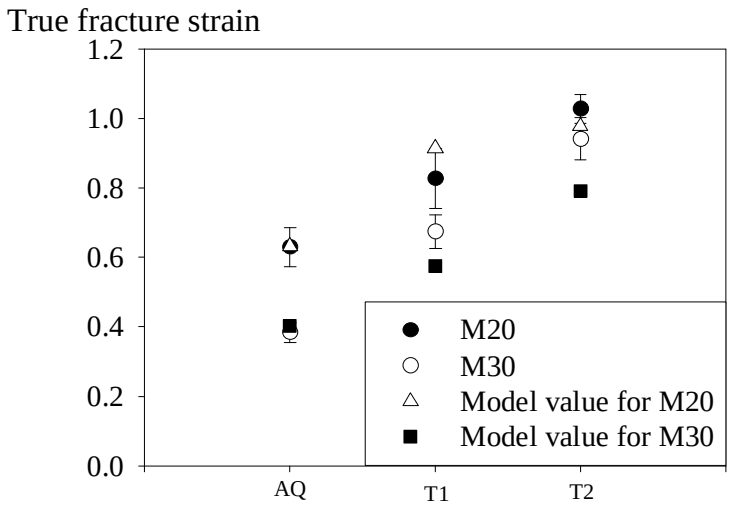

Figure 4: Comparison of the experimental and predicted fracture strains for different conditions and volume fractions of martensite.

4. Discussion of the experimental results

During tempering of DP steels, carbon diffuses from supersaturated martensite particles and forms carbides between martensite needles. This decrease of the martensite C content brings about a decrease of its hardness and affects the mechanical properties. The tensile strength is lower for tempered steel than for as-quenched steel because the martensite strength decreases with C content. Furthermore, yield strength behavior changes after low temperature tempering due to a change in the mobile dislocation density and residual stress as explained by Speich and Miller [2]. Carbide formation induces a volume contraction which decreases the residual stress and increases the yield strength as observed in Fig. 2. The continuous yielding of as-quenched DP steels is also related to the high mobile dislocations density and the high residual stress level [1]. Tempering brings about a decrease of these two parameters and as a consequence a reappearance of a discontinuous yielding (Lüders plateau). The decrease of martensite C content during the tempering also influences the evolution of the true fracture strain. The difference of properties between the two phases is smaller and the strain difference is better accommodated. The hardness variation with the load is due to size effects. Delincé and al. [3] explained that the hardness first decreases with load due to geometrical strain gradient plasticity effects. At larger load, the plastic zone interacts with grain boundaries and the hardness increases.

5. Comparison of experiments with a micromechanics-based model

The model to address the ductile fracture of DP steels integrates a dilatational damage based model with a homogenization scheme. The damage model is based on Gologanu-Leblond-Devaux constitutive law [4, 5], which incorporates void shape effects into the well-known Gurson model for porous ductile metals. It allows a micromechanical description for the three consecutive and interrelated

stages of the ductile fracture, i.e. void nucleation, growth and coalescence, in elasto-plastic materials [6]. The homogenization of the sound material is performed by an incremental formulation of a Mori-Tanaka scheme for elasto-plastic composites [7], and accounts for the load transfer between the two phases, ferrite and martensite. For the details of the micromechanical model, the reader is referred to [8].

The homogenization scheme treats the DP steels as particle (martensite)-matrix (ferrite) composites. The martensite particles are assumed to have a spherical shape. Both phases, ferrite and martensite, are modeled as J_2 elasto-plastic materials, with power-law strain hardening given as

$$\frac{\sigma}{\sigma_0} = \left(1 + \frac{E}{\sigma_0} \varepsilon^{\mathrm{p}} \right)^n , \qquad (2)$$

where E is the Young's modulus, σ_0 is the initial yield strength , n is the strain hardening exponent, and ε^{p} is the accumulated plastic strain. The Young's modulus and the Poisson ratio are taken to be the same for both phases, E=200 GPa and ν=0.3, respectively. Plastic properties are obtained by fitting the stress-strain curves (see Fig. 2) with the Mori-Tanaka scheme. As the hardness of ferrite is almost the same for each DP steel (see Figs. 3c and d), its initial yield strength is also expected to be approximately the same for all six materials, $\sigma_{0\mathrm{F}}$=300 MPa. Figs. 3a and c, however, show that the hardness of martensite is highly sensitive to tempering; hence, its initial yield strength, $\sigma_{0\mathrm{M}}$, was finely tuned for each case separately (see Table 3). It is worth noting that, for each case, the relative initial yield stress of martensite with respect to ferrite, $\sigma_{0\mathrm{M}}/\sigma_{0\mathrm{F}}$, is tuned in a way that it compares well to the value of the relative hardness of martensite with respect to ferrite, $H_{\mathrm{M}}/H_{\mathrm{F}}$, within the limits of the experimental scatter. Finally, the strain hardening exponents that give the best fits for the stress-strain curves irrespective of heat treatments are found to be n_{F}=0.2 and n_{M}=0.3, for ferrite and martensite, respectively. Further studies will be devoted to improve the modeling and identification of the work hardening response of each phase (e.g. [9]).

M20-AQ	M20-T1	M20-T2	M30-AQ	M30-T1	M30-T2
687	370	350	1100	650	400

Table 3a: Initial yield stress values for martensite $\sigma_{0\mathrm{M}}$ (MPa), used in the Mori-Tanaka scheme.

Experimental studies in the literature show that the void nucleation in Dual Phase materials occurs either via the fracture of the stiffer phase or via the decohesion of the interface between the two phases ([10]). Here, we assume that the particle (martensite island) fracture and/or the (martensite-ferrite) interface decohesion start when the maximum principal stress in a particle, $\sigma^{\mathrm{p}}{}_{\text{max-princ}}$, reaches a critical value, σ_{c}, and that void nucleation takes place within a range of critical stress values, $\Delta\sigma_{\mathrm{c}}$, corresponding to a distribution of particles with different size and interface strength. The void nucleation rate in a functional form is taken as

$$\dot{f}_{\text{nuc}} = g\left(\sigma^{\text{p}}{}_{\text{max-princ}}\right)\dot{\sigma}^{\text{p}}{}_{\text{max-princ}},$$
with (3)
$$g\left(\sigma^{\text{p}}{}_{\text{max-princ}}\right) = a_1\left(\sigma^{\text{p}}{}_{\text{max-princ}}\right)^4 + a_2\left(\sigma^{\text{p}}{}_{\text{max-princ}}\right)^2 + a_3,$$

where a_i are chosen to avoid discontinuities in the porosity evolution (see also [8]). The void nucleation parameters (σ_c=1820 MPa and $\Delta\sigma_c$=800 MPa) are identified by fitting the fracture strain ε_f for M20-AQ, and kept the same for the other five cases. Besides, we also assume that both particle fracture and interface decohesion give birth to penny shaped voids with an initial aspect ratio of W_0=0.01. The increase in porosity with void nucleation Δf_{nuc} is related to the particle volume fraction f_{p} and aspect ratio W_{p} via

$$\Delta f_{\text{nuc}} = \frac{\Delta f_{\text{p}} W_0}{W_{\text{p}}}, \tag{4}$$

and the equiaxed martensite particles are assumed to lose all their load carrying capacity after void nucleation.
Another important issue is the evolution of the stress triaxiality T during a tensile test, which locally increases after the onset of necking. The triaxiality evolution is approximated by a linear function:

$$T = \frac{1}{3} + 0.4(\varepsilon_{eq} - \varepsilon_N), \tag{5}$$

where ε_{eq} is the equivalent strain and ε_N is the strain value corresponding to the onset of necking. The onset of coalescence, which is taken to be the fracture strain as well, is decided according to the Thomason criterion (see e.g. [11]).

Figure 5a (5b) shows, as an example, the stress-strain curves given by the micromechanical model for the martensite-ferrite composite and each phase separately for steel M20-AQ (M30-AQ), together with the corresponding experimental stress-strain curves for the four samples analyzed (only up to the onset of necking). There is a very good agreement between the experimental data and the model for steel M20-AQ, whereas the agreement is somewhat poorer for steel M30-AQ, for which the strain hardening behavior is very difficult to capture by the simple power-law given in Eq. 2. It can be seen that after the onset of void nucleation, there is a competition between the strengthening due to strain hardening and softening due to the decrease in the load carrying capacity of the martensite particles.

Figure 4 shows the comparison between the experimental and predicted fracture strains ε_f. Although the model perfectly agrees with the experiments for steels

M20, the discrepancy between the model and the experiments for the strain hardening behavior for steels M30 (see Fig. 5b) represents itself in the predictions for the fracture strain as well.

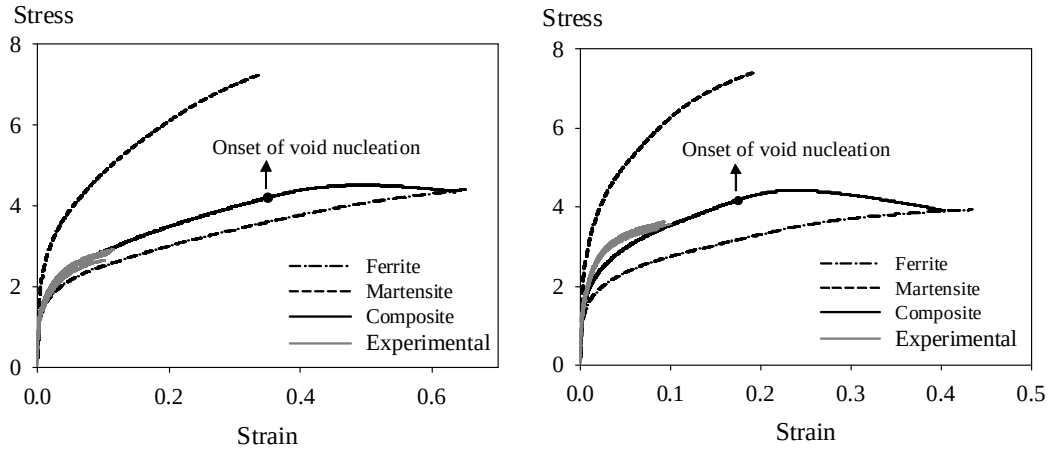

Figure 5: Stress-strain curves given by the micromechanical model for the composite and each phase separately for (a) steel M20-AQ and (b) steel M30-AQ, together with the corresponding experimental stress-strain curves for the four samples analyzed.

6. Conclusion and Perspectives

All the experimental results present in this paper were obtained on two steels with different martensite carbon content. It can be interesting to dissociate the effect of the martensite fraction and the effect of the carbon content of this phase. This parametric study could still improve the understanding of the fracture mechanism. An enhanced understanding of martensite is needed to better represent the mechanical comportment of this phase and consequently of the composite DP steel.

The fracture model presented in section 5 predicts the fracture strain accurately for steels M20, whereas the predictions fall below the experimentally obtained values for steels M30, especially for the tempered samples (see Fig. 4). The model incorporates a very simple power-law strain hardening for both ferrite and martensite (see Eq. 2), which obviously is not enough to capture the complex plastic behavior of these phases. To improve the predictive capacity of the model, a natural extension is therefore to include more physical, microstructure based, strain hardening laws.

7. Acknowledgement

A.-P.P. acknowledges the financial support of ArcelorMittal Research. P.J.J. acknowledges the FNRS (Belgium). This work was partly carried out in the framework of the IAP program of the Belgian State Federal Office for Scientific, Technical and Cultural Affairs, under Contract No. P6/24.

8. References

[1] G.R. Speich, R.L. Miller, Tempering of ferrite-martensite steels, in: Fundamentals of Dual Phase steels, Metallurgical society of AIME, Warrendale, pp279-304.

[2] G.R. Speich, Physical Metallurgy of Dual-Phase Steels, in: Fundamentals of Dual Phase steels, Metallurgical society of AIME, Warrendale, pp3-46.

[3] M. Delincé, P.J. Jacques, T. Pardoen, Separation of size-dependent strengthening contributions in fine grained Dual Phase steels by nanoindentaion, Acta Mater 54 (2006) 3395-3404.

[4] M. Gologanu, J. Leblond, J. Devaux, Approximate models for ductile metals containing non-spherical voids – case of axisymmetric prolate ellipsoidal cavities, J Mech Phys Solids 41 (1993) 1723-1754.

[5] M. Gologanu, J. Leblond, J. Devaux, Approximate models for ductile metals containing non-spherical voids – case of axisymmetric oblate ellipsoidal cavities, ASME J Eng Mater Technol 116 (1994) 290-297.

[6] T. Pardoen, J.W. Hutchinson, An extended model for void growth and coalescence, J Mech Phys Solids 48 (2000) 2467-2512.

[7] I. Doghri, A. Ouaar, Homogenization of two-phase elasto-plastic composite materials and structures Study of tangent operators, cyclic plasticity and numerical algorithms, Int J Solid Structures 40 (2003) 1681-1712.

[8] C. Tekoğlu and T. Pardoen, A micromechanics based model for ductile damage in multiphase and composite metallic alloys combining extended Gurson and homogenization theories, submitted to: Proceedings of the 12th International Conference on Fracture, Ottawa, 2009.

[9] O. Bouaziz, T. Iung, M. Kandel, C. Lecomte, Physical modelling of microstrucutre and mechanical properties of dual-phase steel, J.Phys.IV France 11 (2001), pp 223-231

[10] M.Mazinani, W.J. Poole, Effect of Martensite Plasticity on the Deformation Behavior of a Low-Carbon Dual-Phase steel, Met. trans. 38 (2007) 328-339

[11] P. F. Thomason, Ductile Fracture of Metals, Pergamon Press, Oxford, 1990.